Research Article Vol. 32, No. 12 / 3 Jun 2024 / Optics Express 20432
Optics EXPRESS

Enhancing color saturation in photonic glasses through optimized absorption

GUOTAO ZHANG[1] AND MING XIAO[1,2,*]

[1] College of Polymer Science and Engineering, Sichuan University, Chengdu 610000, China
[2] State Key Laboratory of Polymer Materials Engineering, Sichuan University, Chengdu 610065, China
[*] mingxiao@scu.edu.cn

Abstract: Photonic glasses, isotropically assembled nanoparticles with short-range correlation, can produce angle independent structural colors. They show broader reflectance spectra and lower saturated colors, compared to photonic crystals. Low color saturation creates barriers for photonic glasses to be used for coatings, cosmetics, and colors. Broadband absorbing materials are commonly used to absorb incoherently scattered light to enhance the saturation. However, there is limited understanding on how the absorption quantitatively affects the colors of photonic glasses. To this end, we here use a validated Monte Carlo-based multiple scattering model to investigate how absorption impacts the reflectance spectra in photonic glasses. We show that the color saturation can be maximized with an optimal level of absorption regardless of sample thickness or refractive index contrast between particles and matrix. We quantitatively demonstrate that the multiple scattering is largely reduced with the optimal absorption level and the reflectance is dominantly contributed by the single scattering. The optimal absorption occurs when the sample absorption mean free path is comparable to the transport mean free path, which offers a guidance on how much absorbing material is needed for creating highly saturated photonic glasses. This work will not only pave ways for pushing applications of angle-independent structural colors, but also improve our understanding of light scattering and absorption in short-range correlated disordered systems.

© 2024 Optica Publishing Group under the terms of the Optica Open Access Publishing Agreement

1. Introduction

Photonic glasses are typically isotropic assemblies of particles or voids of hundreds of nanometers with short-range order. They are an intermediate state between totally random and crystalline structures. Their short-range correlation leads to selective backscattering of specific wavelengths. Early studies on photonic glasses focused on the tuning of photonic bandgap in photonic crystals with increased disorder [1,2] or the light diffusion properties in multiple scattering systems [3,4]. After the surprising findings that the angle independent blue color of some bird feathers [5–7] was produced by the disordered nanostructures rather than pigments, physicists and biologists have worked together to reveal that photonic glasses can produce structural colors in the single scattering or weak multiple scattering regime. This has recently motivated materials scientists to control the packing of colloidal particles to form photonic glasses for various applications, such as displays, painting, and cosmetics [8–10].

The colors of photonic glasses are much less saturated compared to photonic crystals, limiting their applications. A common way to increase color saturation is to dope photonic assemblies with broadband absorbers, which do not show any absorption peaks and absorb light similarly across visible wavelengths. Typical broadband absorbers are carbon black (CB) [10–13], natural or synthetic melanin [14–18], carbon nanotube [19], and graphene [20–22]. These absorbers reduce the penetration depth of light through the sample and reduce reflectance across the spectrum. Another way of increasing color saturation is to add the absorption outside the material, such as using a black quartz as the substrate of the photonic film [23]. Compared to adding absorption into photonic materials, the underlying mechanism in this approach is straightforward without

#516278 https://doi.org/10.1364/OE.516278
Journal © 2024 Received 18 Dec 2023; revised 27 Apr 2024; accepted 1 May 2024; published 20 May 2024

Optics EXPRESS

involving complicated interaction of multiple scattering and absorption. The transmitted light is absorbed by the absorbing substrate, effectively reducing the reflected light from the substrate and transmitted light from backside of the photonic film.

There are different approaches to add absorption into photonic glasses, either by blending absorbing materials to make the matrix absorbing or directly assembling absorbing particles. Absorbers can be incorporated into matrix or coated onto the surface of nanoparticles. Takeoka and colleagues prepared structurally colored films by spraying solutions of silica nanoparticles. The colors became more vivid when mixing the silica solutions with enough amount of carbon black [10]. Chu et al. increased color saturation of films of hollow titanium dioxide nanoparticles by adding a small amount of cuttlefish ink nanoparticles [14]. In contrast to previous two examples where absorbers were placed in the matrix, Xiao and coworkers used an evaporative assembly method to produce photonic films from polydopamine nanoparticles [24]. The intrinsic absorption of polydopamine improved the color saturation. Wang et al. prepared responsive structurally colored films from assembling lignin colloidal nanoparticles [25]. Similar to polydopamine, lignin nanoparticles enhanced the color saturation through their broad absorption of the visible light.

The use of intrinsic absorbing nanoparticles will cause too much absorption, making samples black, when they are packed too thick. To avoid the issue, one can coat a thin layer of absorbing materials onto nonabsorbing nanoparticles. Kawamura and co-workers [18] coated the surface of the nanoparticles with polydopamine to obtain core-shell nanoparticles. The absorption of the polydopamine shell increased the saturation of structurally colored films of core-shell nanoparticles. Lin et al. functionalized the surface of polystyrene nanoparticles with xanthommatin to make absorbing particles and they mixed polystyrene particles with 0% to 25% w/w xanthommatin modified particles to enhance saturation of bi-disperse photonic films [26].

Despite these reported experiments where absorbers are used to enhance saturation, it is unclear how absorption quantitatively affects color saturation of photonic glasses and how much absorption is needed to obtain the best saturation. Experimentally, it is challenging to quantitatively control the amounts of absorbers without affecting the packing of particles in photonic glasses. In theory, it is a nontrivial task to account for absorption in the calculation. There are several reported models or approaches to predict the structural colors of photonic glasses, such as single scattering model [27], double scattering model [6,28], Ewald sphere construction method [29,30], energy-density coherent-potential approximation [31,32], but these methods can rarely be applied to systems with absorption. Numerical calculations such as finite-difference time-domain (FDTD) [33,34] can deal with absorption, but they require inputs of coordinates of assembled particles, which are often generated from simulations. In addition, FDTD calculations need high computational costs.

Recently, the Manoharan group have developed a Monte Carlo method to simulate the multiple scattering in photonic glasses [35–37]. This multiple scattering model works well with absorption and successfully predicts the structural color of photonic glasses with different concentrations of carbon black (0.03 - 0.1% w/w) [36]. Here we use the multiple scattering model to explore how absorption affects color saturation of photonic glasses quantitatively. We investigate the spectra and colors of photonic glasses with absorption placed in the matrix and different index contrasts between nanoparticles and matrix (- 0.45 to + 0.45). With the increase of absorption, the color saturation of photonic glasses increases first and then decreases. The same trend is observed for photonic glasses with different index contrasts. When the color saturation reaches its maximum, the corresponding absorption mean free path is comparable to the transport mean free path and the colors primarily come from the single scattering. This finding not only provides a design rule of fabricating highly saturated photonic glasses, but also increases our understanding of interplay of scattering and absorption in correlated disordered photonic systems.

Optics EXPRESS

2. Methods

2.1. Multiple scattering model

We use the Monte Carlo multiple scattering model developed by the Manoharan group [36–38], for which open-source code is available on GitHub [39]. This model simulates how light interacts with short-correlated disordered materials, typically a film composed of spherical nanoparticles or voids inside a matrix. The inputs of the simulations are experimentally measurable parameters, including particle volume fraction, particle refractive index, particle size, matrix refractive index, and sample thickness. With these parameters, we can calculate the scattering and absorption of nanoparticles and voids by assuming the sample as a homogeneous, effective medium. The effective refractive index may affect the scattering amplitude and phase [40,41]. Stephenson and co-authors demonstrate it is reasonable to use effective refractive index for both form factor and structure factor in many photonic glass systems [38]. The form factor is calculated using Mie theory [42] and the structure factor is described by Percus-Yevick approximation, which is a function of volume fraction [37].

In a typical simulation, photon packets are set to enter the sample at each wavelength, and photons undergo successive scattering within the sample following the principle of single scattering before exiting the sample boundary. We sample the distances between each scattering from an exponential probability distribution called step size distribution. This distribution is based on the Beer-Lambert law:

$$P(\text{step}) = \frac{1}{l_{\text{sca}}} e^{(-\text{step}/l_{\text{sca}})} \tag{1}$$

The mean of this distribution is scattering mean free path l_{sca}, which is a function of number density of nanoparticles (ρ) and total scattering cross section of the sample (σ_{sca}),

$$l_{\text{sca}} = \frac{1}{\rho \sigma_{\text{sca}}} \tag{2}$$

The scattering directions follow a phase function that is calculated with consideration of both form factor (F) and structure factor (S) [27]:

$$P(\theta) = \frac{FS}{\sigma_{\text{sca}}} \tag{3}$$

The degree of absorption is determined by the imaginary part of the refractive index of the materials. We use an appropriate Mie solution to account for absorption in the photonic glasses, as well described by Hwang and colleagues [36]. When the particle or matrix has complex refractive indices, the total cross-section is obtained by integrating differential scattering cross-section at the surface of particles. Then absorption between adjacent scattering events is calculated based on Beer-Lambert law, which reduces the weight of each photon packet:

$$W = W_i e^{-\text{step}/l_{\text{a}}} \tag{4}$$

where $l_{\text{a}} = \lambda_0 / 4\pi k_{\text{sample}}$ is the absorption mean free path. λ_0 is the wavelength in the vacuum and k_{sample} is the effective imaginary index of the sample. This approach of modeling absorption leads to great agreements between predicted and measured spectra as shown by Manoharan group [36,38].

The reflection or transmission spectrum can be calculated by counting the percentages of photons exiting the surface or the bottom of the sample at each wavelength. Typically, we collect all photons scattered to the whole back hemisphere to calculate reflectance. Since trajectories of all photon packets are saved, we can identify how many times the photons get scattered

Optics EXPRESS

before exiting the sample and calculate the contribution of different scattering modes to the total reflectance spectrum.

Silica nanoparticles are widely used in various fields due to their convenient synthesis and excellent stability. They are more stable in organic resins than polymeric nanoparticles, such as polystyrene or poly(methyl acrylate). Considering the feasibility of reproducing the simulation conditions in future experiments, in our simulations we choose silica nanoparticles (real index = 1.45) embedded in matrices with different refractive indices from 1.0 to 1.9. We tune the absorption by varying imaginary index of particles or matrix.

2.2. Calculation of color saturation

Saturation is a quantity describing the colorfulness of colorants, which can represent the purity of the color [43]. To quantify how the simulated spectra of photonic glasses are perceived by human visions, we use the CIELAB (CIE 1976) color space with a standard setting: a standard observer (CIE 1931 2°) and a standard D65 illuminant. Following reported procedures [37], we first calculate three color values, L^*, a^*, and b^* from simulated reflectance spectra. The color saturation (s) is then calculated as,

$$s = \sqrt{a^{*2} + b^{*2}}/L^* \tag{5}$$

where L^* is the lightness of the color, which is a measure for reflectance of a non-self-luminous colorant [43], a^* represents green to red contribution, and b^* represents blue to yellow contribution.

2.3. Fabrication of photonic glass films with tuned absorption

We first synthesized silica nanoparticles following a modified Stöber method [44]. At 20 °C, a mixture of 16 mL methanol (AR, Chron Chemicals), 25 mL deionized water, and 7 mL ammonia solution (28%, Chron Chemicals) were poured into a flask with magnetic stirring. After 20 minutes, a mixture of 4.5 mL tetraethyl orthosilicate (AR, Chron Chemicals) and 45.5 mL methanol was quickly added to the flask. After stirring for 2 hrs, the products were centrifuged and washed to obtain silica nanoparticles of 218 nm.

We drop cast solutions of silica nanoparticles to make photonic glass samples. We mixed 10% w/w ethanol solutions of silica nanoparticles and 0.1% w/w ethanol solutions of carbon black (AR, Tanfeng Tech. Inc). We adjusted the absorption by changing the amount of carbon black solution. The total volume of ethanol in the mixed solution was fixed by adding additional ethanol, which did not change the volume of nanoparticles. To make photonic glass films, we then added 150 μL of the mixture into the home-made groove on a glass plate that was placed on a heating stage to accelerate evaporation. After ethanol evaporated, we obtained photonic glass films from precipitation of silica nanoparticles with a small amount of carbon black. We then measured the reflectance spectra of samples using a microscope (Nikon LV100 ND) connected to an optic fiber spectrometer (Idea PG2000). The spectra were taken using a 10x objective lens and a polytetrafluoroethylene whiteboard (Thorlabs, PMR10P1) as the white reference. The surface morphology of the sample was characterized using scanning electron microscopy (German ZEISS Gemini SEM 300).

2.4. Polarization measurements

Following a reported protocol [28,35], we measured the polarization spectrum of the sample using a UV-vis near-infrared spectrophotometer (Cary 5000) with the detector angle $\theta = 20°$. We measured both co-polarized and cross-polarized spectra. The co-polarized spectrum includes all singly scattered light and multiply scattered light returning to the initial polarization direction, while the cross-polarized spectrum contains only multiply scattered light that changes polarization direction by 90°.

Optics EXPRESS

To measure unpolarized spectrum, we placed a polarizer between light source and sample and calculated the unpolarized reflectance as:

$$R_{\text{unpolarized}} = \frac{I_{\text{s,sample}}}{I_{\text{s,blank}}} \tag{6}$$

where $I_{\text{s,blank}}$ is the light intensity after going through a polarizer without a sample and $I_{\text{s,sample}}$ is the intensity of light scattered with a polarizer between the light source and the sample.

The co-polarized and cross-polarized reflectance were measured by adding another polarizer between the sample and the detector. When the second polarizer was parallel with the first polarizer, we measured the scattered intensity as $I_{\text{ss,sample}}$ (Fig. 1(a)); and when the second polarizer was perpendicular to the first polarizer, we measured the scattered intensity as $I_{\text{sp,sample}}$ (Fig. 1(b)). Considering the light intensity decreased after passing through the second polarizer, we corrected this loss to calculate co-polarized and cross-polarized reflectance using transmittance (T) of the second polarizer:

$$R_{\text{co}} = \frac{I_{\text{ss,sample}}}{I_{\text{s,blank}}T} \tag{7}$$

$$R_{\text{cr}} = \frac{I_{\text{sp,sample}}}{I_{\text{s,blank}}T} \tag{8}$$

$$T = \frac{I_{\text{ss,blank}}}{I_{\text{s,blank}}} \tag{9}$$

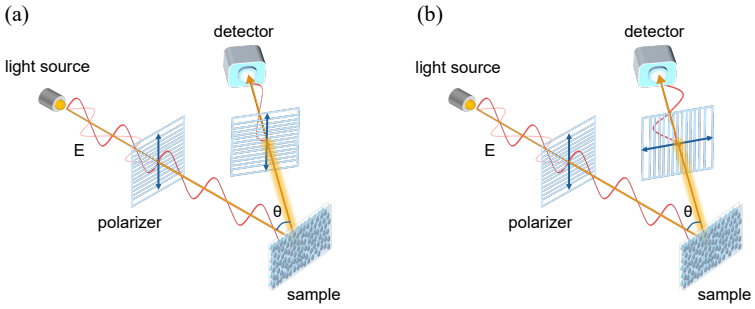

Fig. 1. Schematic of the polarization measurement setup. The light source is illuminated vertically onto the sample through a linear polarizer, and the scattered light is collected by the detector at $\theta = 20°$ through another polarizer. (a) Co-polarized measurement with two polarizer of the same polarization direction. (b) Cross-polarized measurement with two polarizers of different polarization directions. The blue arrow indicates the polarization direction.

Considering any light scattered more than once is randomly polarized, we can assume half of the multiply scattered light is collected by the detector through two cross polarizers and the other half is probed through two parallel polarizers, and all the singly scattered light is probed through two parallel polarizers [35]. The singly scattered light doesn't change polarization direction. We then used Eq. (10) and Eq. (11) to get a rough estimate of the fraction of single and multiple scattering in the reflectance spectrum:

$$R_{\text{single-scat}} = R_{\text{co}} - R_{\text{cr}} \tag{10}$$

$$R_{\text{multiple-scat}} = 2R_{\text{cr}} \tag{11}$$

Optics EXPRESS

3. Results and discussion

3.1. Placement and variation of absorption

The Monte Carlo-based multiple scattering model can deal with the multiple scattering in photonic glasses, namely disorderly assembled colloidal particles with short-range correlations. We can adjust the imaginary index of the particles or matrix to account for absorption in the system. To investigate if where to place absorption affects the reflectance spectra or colors, we simulate reflectance spectra from two photonic glass samples that are silica particles assembled in water with the same thickness (200 μm), volume fraction (60%), and particle diameter (220 nm). We put absorption either to silica particles or water matrix by adding imaginary refractive indices in the calculations. If we set particles and matrix to have the same imaginary index in these two samples, the sample with absorbing particles will absorb much more than the sample with absorbing matrix. This is because the particle volume fraction is larger than the matrix. To make fair comparisons, we not only need to keep the same real indices of matrix and particles in two samples, but also must keep both samples with the same effective complex index to have the same degree of absorption. When setting the imaginary index of the particles in one sample, we can calculate the matrix imaginary index of the other sample using the Bruggeman effective medium theory [45],

$$f\frac{n_{\text{particle}}^2 - n_{\text{sample}}^2}{n_{\text{particle}}^2 + 2n_{\text{sample}}^2} + (1-f)\frac{n_{\text{matrix}}^2 - n_{\text{sample}}^2}{n_{\text{matrix}}^2 + 2n_{\text{sample}}^2} = 0 \tag{12}$$

where n_{sample} is the effective index of sample, n_{matrix} is the index of matrix, n_{particle} is the index of particles, and f is the volume fraction of particles. In one photonic glass sample, we set the particle index to be $1.45 + 1.11 \times 10^{-5}j$ and matrix index 1.33. We calculate the other sample to have particle index of 1.45 and matrix of $1.33 + 1.65 \times 10^{-5}j$ by keeping both samples the same complex effective refractive index. As shown in Fig. 2, both reflectance and transmittance spectra are almost the same. Thus, in the multiple scattering model, the reflectance spectra or colors do not depend on whether we put absorption to particles or matrix as long as the effective refractive index of the sample is fixed.

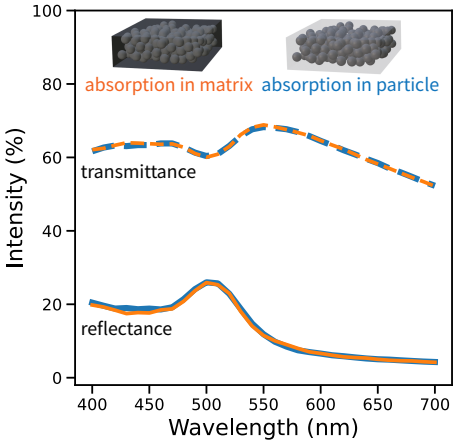

Fig. 2. Calculated reflectance (solid line) and transmittance (dashed line) spectra for two samples with the same complex effective refractive index. One sample has absorption in particles (blue curves) and the other has absorption in matrix (orange curves). Both samples have particle radii of 110 nm, volume fraction of 60%, and thickness of 200 μm.

Optics EXPRESS

It is more experimentally feasible to add absorbers into the matrix compared to adding absorption to particles, and we here add absorption to the matrix to simulate how absorption affects the saturation of the photonic glasses. In the simulations, we adjust the imaginary index of the matrix, k_{matrix}, from 0 to 0.050. At the upper limit of absorption, the effective imaginary index of the sample (60% v/v particles) is $k_{\text{sample}} = 0.021$, and the absorption mean free path is $l_{\text{a}} = \lambda/4\pi k_{\text{sample}} = 2.4$ μm at 600 nm. For a 200 μm sample, we calculate that the transmittance of the sample is on the order of 10^{-37} according to Beer–Lambert law, and its absorptance is almost 100% when ignoring Fresnel reflection. When absorption is above this upper limit, the sample appears entirely black without any other colors. Thus, we restrict our simulations within this absorption range ($k_{\text{sample}} \leq 0.021$).

3.2. Saturation with absorption

To understand how absorption quantitatively affects color saturation in photonic glasses, we firstly calculate photonic glass samples that are short-range correlated nanoparticles with real index of 1.45 (similar to index of silica particles) embedded in matrix. The nanoparticles stack as a hard-sphere packing, described by Percus-Yevick structure factor. The particle volume fraction is 60%, the sample thickness is 200 μm, and the imaginary index of the matrix is varied from 0 to 0.05. To quantify the degree of absorption, we calculate the average absorption coefficient α (inverse of average absorption mean free path from 400 nm to 700 nm, which is the typical wavelength range of human vision) of the sample to be $0-4.8\times10^{-1}\,\mu\text{m}^{-1}$. The larger absorption coefficient represents higher degree of absorption.

To quantify how absorption affects the colors in systems, we calculate lightness and color saturation from simulated reflectance spectra based on CIELAB standard. When the absorption coefficient increases (Fig. 3(a)), the reflectance decreases and color lightness decreases (Fig. S1). The color saturation increases first and then decreases down to almost zero when absorption coefficient is too high. Color saturation can be optimized with an appropriate absorption coefficient.

Color saturation results from the combined influence of all visible wavelengths. To investigate the impact of absorption at different wavelengths, we calculate the decreased reflectance ratio for different absorption coefficient,

$$\overline{R} = (R_0 - R)/R_0 \tag{13}$$

where R is the reflectance with absorption and R_0 is the reflectance without absorption. A larger $\overline{R}$ represents a larger decrease in the reflectance. $\overline{R}$ is zero when there is no absorption, and it increases as absorption increases (Fig. 3(b)). For moderate absorption, the $\overline{R}$ has a dip at the reflectance peak wavelength, indicating the reflectance around the peak wavelengths decreases much less than that at off-peak wavelengths. Thus adding absorption can increase contrast between reflectance peak and off-peak intensities, thus leading to higher color saturation. We find this is consistent to experimental reflectance data by Takeoka [10], by plotting the decreased reflectance ratio with different concentrations of carbon black added to photonic glass films (Fig. S2).

Multiple scattering has tremendous effects on the colors in photonic glasses [35]. When the sample thickness increases, the multiple scattering becomes stronger. We vary the sample thickness to different proportions of average transport mean free path from $\overline{l^*}$ to $\overline{10l^*}$. We compute reflectance spectra for samples with different thicknesses and varying absorption coefficients. As shown in Fig. S3(a), reflectance increases with the sample thickness when the absorption is weak ($k_{\text{matrix}} = 1.8\times10^{-6}$). With increasing absorption, the color saturation first increases and then decreases after reaching a maximum (Fig. 4). The absorption for the maximum saturation (we term it the optimal absorption coefficient) stays the same ($\alpha = 2.6\times10^{-2}$ μm^{-1}) regardless of the thickness. With optimal absorption, the reflectance stays the same for different thicknesses (Fig. S3(b)).

Optics EXPRESS

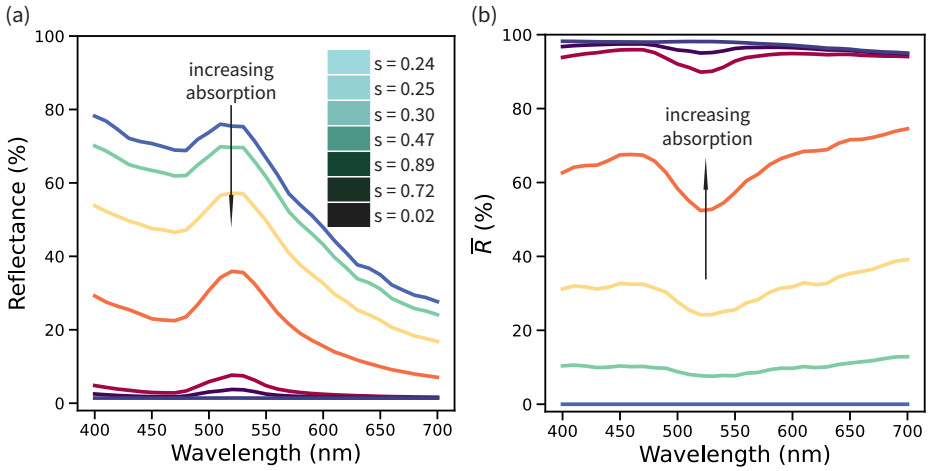

Fig. 3. (a) Reflectance spectra of photonic glasses with different degrees of absorption. The absorption coefficients of the samples are 0 μm^{-1}, 1.6×10^{-4} μm^{-1}, 6.8×10^{-4} μm^{-1}, 2.9×10^{-3} μm^{-1}, 2.6×10^{-2} μm^{-1}, 5.4×10^{-2} μm^{-1}, 4.8×10^{-1} μm^{-1} from the top to the bottom spectrum. Insets show color swatches and saturation calculated from reflectance spectra using Eq. (5). (b) Plots of the decreased reflectance ratio ($\overline{R} = (R_0 - R)/R_0$) with wavelengths show that absorption has wavelength-dependent attenuation effects on reflectance. Simulation parameters: $n_{\text{particle}} = 1.45$, $n_{\text{matrix}} = 1$, k_{matrix} varies from 0 to 0.05, the volume fraction is 60%, and the sample thickness is 200 μm.

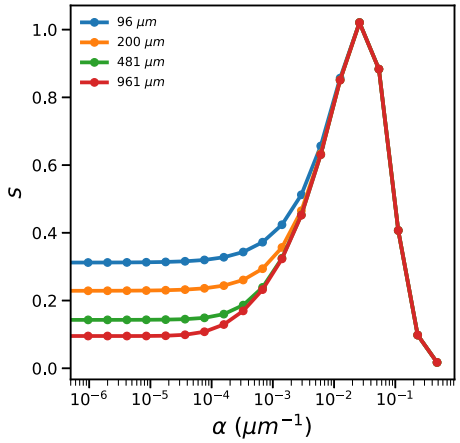

Fig. 4. Color saturation versus absorption coefficient when the sample thickness varies from 96 μm ($\overline{l^*}$), 200 μm ($2.08\overline{l^*}$), and 481 μm ($5\overline{l^*}$), to 961 μm ($10\overline{l^*}$). $\overline{l^*}$ is the average transport mean free path over 400 - 700 nm. Simulation parameters: $n_{\text{particle}} = 1.45$, $n_{\text{matrix}} = 1$, k_{matrix} changes from 0 to 0.05, the volume fraction is 60%, and the particle radius is 125 nm.

Optics EXPRESS

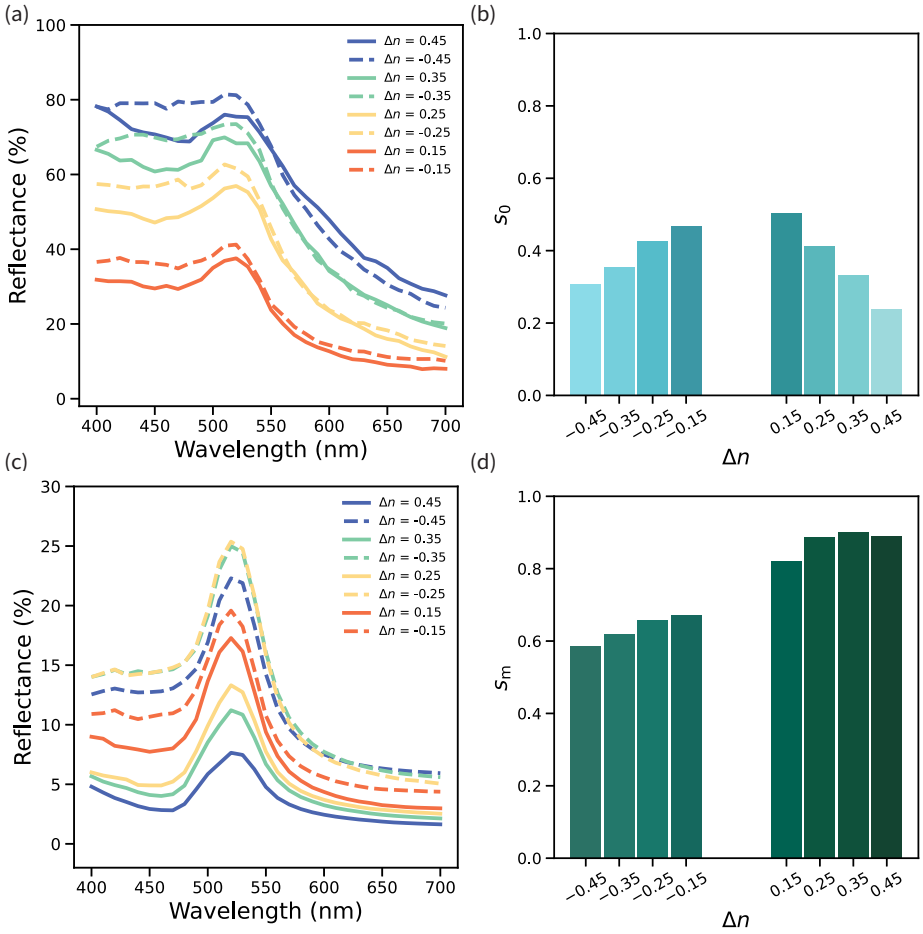

Fig. 5. The effect index contrasts on reflectance spectra and color saturation when there is no absorption or optimal absorption. Reflectance spectra of different index contrasts (Δn) (a) without absorption and (c) with optimal absorption coefficient. To keep the reflectance peak at 520 nm for different index contrasts, we vary radius (r) by keeping the product of n_{sample} and r the same. Bar plots of (b) color saturation without absorption (s_0) and (d) maximum color saturation (s_{m}) versus the index contrast. Insets are color swatches calculated based on the corresponding reflectance spectra. Simulation parameters: $n_{\text{particle}} = 1.45$, n_{matrix} changes from 1.0 to 1.9, the volume fraction is 60%, and the sample thickness is 200 μm. When $\Delta n = 0.45$, the radius of particle is 125 nm.

In addition to the sample thickness, the degree of multiple scattering highly depends on the refractive index difference between the particles and matrix ($\Delta n = n_{\text{particle}} - n_{\text{matrix}}$). We adjust the real indices of the matrix from 1.0 to 1.9 with an increment of 0.10, making the absolute index contrast ($|\Delta n|$) between the particle and the matrix up to 0.45. When the particle real index is larger than that of the matrix, Δn is positive and we refer to the samples as "direct photonic glasses". The samples with negative Δn are referred to as "inverse photonic glasses".

The scattering strength (λ/l^*), which is a ratio of the wavelength to the transport mean free path, can represent the degree of scattering [28]. The scattering strength increases with $|\Delta n|$ (Fig. S4). The largest scattering strength at $|\Delta n| = 0.45$ is about 0.035, much less than 2π, and we can ignore the near coupling effect or Anderson localization [36,46]. When $|\Delta n|$ is 0.05, the

Optics EXPRESS

scattering strength is smaller than 0.001 and the curve is almost flat without obvious resonance peaks. In addition, the transport mean free path is at least ten times larger than the sample thickness as shown in Fig. S5, indicating the single scattering dominates over multiple scattering when $|\Delta n| = 0.05$. Thus, we consider 0.15 as the lower limit for $|\Delta n|$.

When varying the index contrast, the reflectance peak will shift. To have fair comparisons on how absorption affects color saturation of photonic glasses with different index contrasts, we adjust the particle radius to fix the reflectance peaks at the same wavelengths. The particle radius is set based on the equation $n_{\text{sample}} \times r = \text{constant}$. Where n_{sample} is calculated using Bruggeman effective medium theory. As shown in Fig. 5(a), the reflectance peaks are kept at around 520 nm for different index contrasts. As $|\Delta n|$ increases from 0.15 to 0.45, the reflectance increases from about 40% to about 80% when there is no absorption. For the same $|\Delta n|$, direct samples ($\Delta n>0$) show lower reflectance than inverse ones ($\Delta n<0$). With plotting the color saturation with index contrast, we find the saturation decreases with the increase of $|\Delta n|$ when there is no absorption (Fig. 5(b)).

When adding absorption into the matrix, the reflectance decreases and the reflectance peak narrows for all index contrasts (Fig. S6). With further increase of absorption, the reflectance goes close to zero. As shown in Fig. S7, the lightness of both direct and inverse samples first doesn't change much with absorption and then sharply drops after the absorption coefficient is larger than 10^{-4} μm^{-1}. When absorption is too high ($\alpha>10^{-1}$ μm^{-1}), the lightness decreases little likely because the reflectance is already very low.

The color saturation first increases with the absorption and then reaches a maximum for all index contrasts (Fig. 6). When the absorption is too high, the sample turns black and the saturation decreases to zero. With $|\Delta n|$ increasing from 0.25 to 0.45, the optimal absorption coefficient increases from 1.3×10^{-3} μm^{-1} to 2.6×10^{-2} μm^{-1}. When $|\Delta n|$ is smaller than 0.25, the optimal absorption coefficient is similar for both direct and inverse samples. With $|\Delta n| \geq 0.25$, direct samples have a larger optimal absorption coefficient than inverse ones.

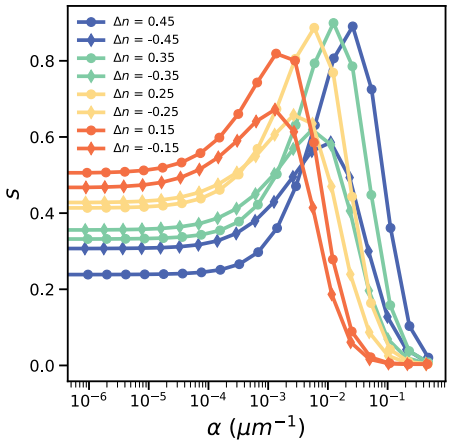

Fig. 6. Color saturation changes with the sample absorption coefficient for different index contrasts. Circle and diamond markers represent direct and inverse samples. The color of curves represents the same $|\Delta n|$. Simulations parameters: $n_{\text{particle}} = 1.45$, n_{matrix} varies from 1.0 to 1.9, k_{matrix} changes from 0 to 0.05, the volume fraction is 60%, and the sample thickness is 200 μm.

Figure 5(c) shows reflectance spectra with optimal absorption. Off-peak reflectance at short wavelengths largely decreases to much lower than the reflectance peaks. The reflectance for inverse samples is much larger than that for direct ones when $|\Delta n|$ is the same. The maximum

Optics EXPRESS

color saturation increases as Δn rises from −0.45 to 0.35 and plateaus thereafter (Fig. 5(d)). This suggests direct photonic glasses make more saturated colors than inverse ones if we fix the reflectance peak and add the optimal absorption. This is likely because the negative index contrast in inverse samples leads to stronger multiple scattering at short wavelengths before peak positions and colors are less saturated.

By calculating the ratio of the maximum saturation with optimal absorption (s_m) to the saturation without absorption (s_0), s_m/s_0, we can quantify the degree of enhancement of absorption on color saturation. As $|\Delta n|$ increases from 0.15 to 0.45, s_m/s_0 of direct samples increases from 1.6 to 3.7 while it increases from 1.4 to 1.9 for inverse samples (Fig. S8(a)). This demonstrate that the absorption can increase color saturation of direct photonic glasses more significantly than that of inverse ones.

3.3. Mechanism behind the optimal absorption

To investigate the mechanism behind the optimal absorption at different index contrasts, we compare the transport mean free path l^* and optimal absorption mean free path $l_{\text{a-opt}}$. $l_{\text{a-opt}}$ and l^* intersect at the visible wavelengths for different index contrasts (Fig. S9). For direct photonic glasses, the position of intersection between $l_{\text{a-opt}}$ and l^* shifts from 581 nm to 542 nm when Δn increases from 0.15 to 0.45 (Fig. S9(a)). For inverse samples, the intersecting wavelength shifts from 580 nm to 600 nm when Δn varies from - 0.15 to - 0.25, and then shifts from 600 nm to 580 nm when Δn changes from - 0.25 to - 0.45 (Fig. S9(b)). When Δn = 0.45, $l_{\text{a-opt}}$ and l^* have extra two intersection points at low wavelengths before the reflectance peak position. The intersection between $l_{\text{a-opt}}$ and l^* suggests they are within the same order of magnitude.

To quantitatively compare $l_{\text{a-opt}}$, and l^*, we average these two lengths over 400 - 700 nm. As shown in Fig. 7, the average optimal absorption mean free path ($\overline{l_{\text{a-opt}}}$) and the average transport mean free path ($\overline{l^*}$) both decrease when $|\Delta n|$ increases from 0.15 to 0.45. This suggests that as $|\Delta n|$ increases, the multiple scattering of the sample becomes stronger and the sample needs more absorption to achieve the optimal saturation. $\overline{l_{\text{a-opt}}}$ decreases from 831 μm to 97.0 μm for inverse structures and decreases from 798 μm to 41.6 μm for direct structures when $|\Delta n|$ raises from 0.15 to 0.45. The direct structures need more absorption than the inverse ones when the index contrast is high.

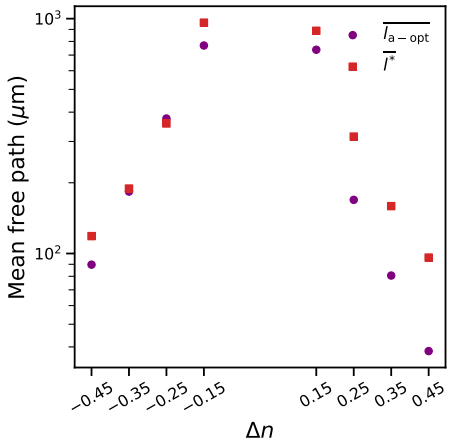

Fig. 7. The average optimal absorption mean free path ($\overline{l_{\text{a-opt}}}$) and the average transport mean free path ($\overline{l^*}$) for different index contrasts when reflectance peak is at about 520 nm.

Optics EXPRESS

When $\overline{l_{\text{a-opt}}}$ is similar to $\overline{l^*}$, the sample achieves the optimal saturation. This physically means light will get absorbed before the light propagation direction gets randomized. To address why these two lengths are comparable to each other, we track how many times the reflected photons are scattered before exiting the sample in the simulation. We group triply and higher order scattering as the multiple scattering. When there is no absorption, the multiple scattering intensity is larger than the single scattering and double scattering (Fig. 8(a)). The reflectance peak position aligns well with the single scattering peak. This means the reflectance peak comes from the single scattering and gets largely broadened by the multiple scattering. With the optimal saturation, the reflectance spectrum (Fig. 8(b)) is primarily contributed by the single scattering, suggesting the multiple scattering is largely reduced by absorption.

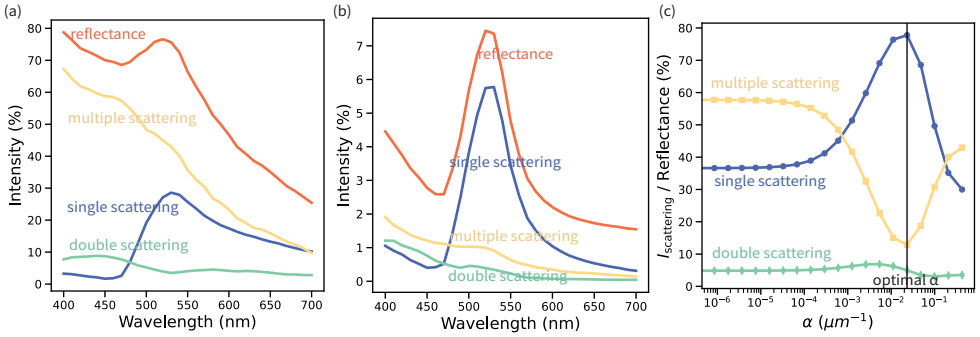

Fig. 8. The composition of reflectance spectrum (a) without absorption and (b) with optimal absorption. (c) The percentage of intensity of different scattering modes to the reflectance ($I_{\text{scattering}}$/Reflectance) varies with absorption coefficients at reflectance peak position. Simulation parameters: $n_{\text{particle}} = 1.45$, $n_{\text{matrix}} = 1$, the volume fraction is 60%, and the sample thickness is 200 μm.

To assess the contribution of different scattering modes, we calculate the percentage of intensity of different scattering to the reflectance ($I_{\text{scattering}}$/Reflectance) at different levels of absorption. As shown in Fig. 8(c), with the increase of absorption, the percentage of single scattering and double scattering first increases and then decreases, while the percentage of multiple scattering first decreases and then increases. Optimal absorption occurs when the single scattering percentage reaches a maximum and the multiple scattering percentage goes to a minimum. The same trend is observed in samples of different refractive index contrasts (Fig. S10).

3.4. *Design of photonic glasses with optimized saturation*

We demonstrate that highly saturated photonic glasses can be made by adding suitable amount of absorption into the matrix, which makes the sample absorption mean free path comparable to the transport mean free path. This provides a design rule on how much absorption should be added to create highly saturated photonic glasses. As shown in Fig. 9, we start by calculating l^* using the experimentally measurable parameters including particle refractive index (n_{particle}), particle radius (r), particle volume fraction (ϕ), and matrix refractive index (n_{matrix}). We then set the average absorption mean free path to the average transport mean free path over 400-700 nm, $\overline{l_{\text{a}}} = \overline{l^*}$, which leads us to calculate the imaginary refractive index of the sample, $k_{\text{sample}} = \lambda/4\pi\overline{l_{\text{a}}}$. Using Bruggeman equation, we can calculate how much absorption is needed for the matrix or the particles to achieve optimized saturation.

We take the sample in Fig. 3 for an example, where silica nanoparticles of 250 nm are packed in air with volume fraction of 60%. Using these parameters, we first calculate $\overline{l^*} = 96.1$ μm and obtain the imaginary refractive index of the sample, $k_{\text{sample}} = \lambda/4\pi\overline{l_{\text{a}}} = 4.55 \times 10^{-4}$ at 550 nm by

Optics EXPRESS

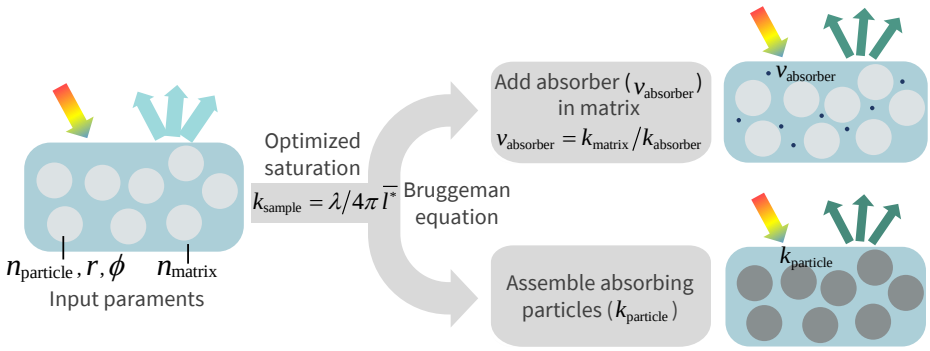

Fig. 9. Workflow to make photonic glasses with optimized color saturation either by adding an appropriate amount of absorber into the matrix or by assembling absorbing particles with desired imaginary index.

setting $\bar{l}_a = \bar{l}^*$. We then compute the imaginary index of the matrix using Bruggeman equation, $k_{matrix} = 1.08 \times 10^{-3}$. Considering carbon black is widely used to enhance color saturation of photonic glasses [10–13], we here choose to use carbon black ($k_{CB} = 0.44$) [47,48] as the absorption material to incorporate into the matrix. The required volume percentage of carbon black within the matrix is calculated using the equation, $v_{CB} = k_{matrix}/k_{CB} = 2.46‰$. When the matrix is not air, we need improve its dispersion in solvents by surface modification of carbon black through physisorption, chemisorption, oxygen plasma, or polymer grafting [49,50].

In addition to adding absorbers to the matrix, one can also use absorbing particles to make highly saturated photonic glasses. With the sample imaginary index $k_{sample} = 4.55 \times 10^{-4}$ as calculated above, we can determine the required particle imaginary index to be $k_{particle} = 7.81 \times 10^{-4}$. When these particles assemble to photonic glasses, high saturation is achieved (Fig. S11).

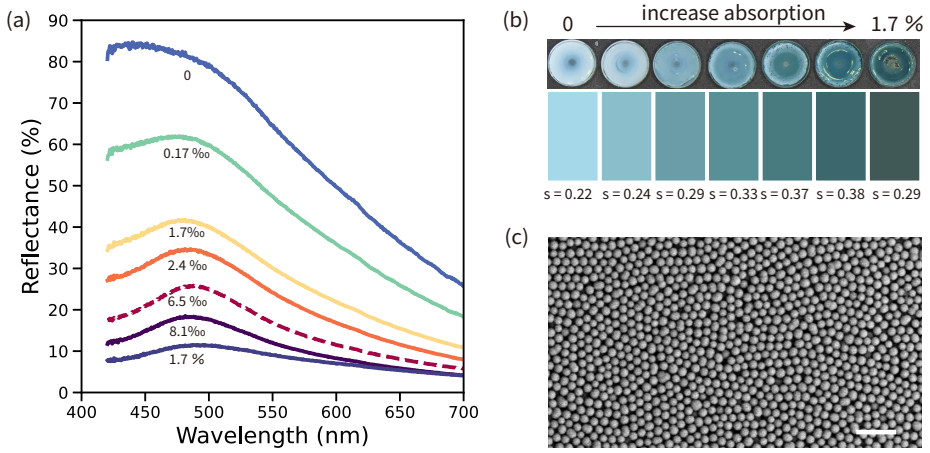

Fig. 10. (a) Reflectance spectra of photonic glass samples with different concentrations of carbon black. The volume percentage of carbon black to the matrix (v_{CB}) varies from 0, 0.17‰, 1.7‰, 2.4‰, 6.5‰, 8.1‰, up to 1.7%. The amount of carbon black added in the dashed line is guided by our design rule. (b) The sample photos (top) and color swatches and saturation calculated from reflectance spectra (bottom). (c) The SEM image of the sample with $v_{CB} = 6.5‰$. Scale bar is 1 μm.

Optics EXPRESS

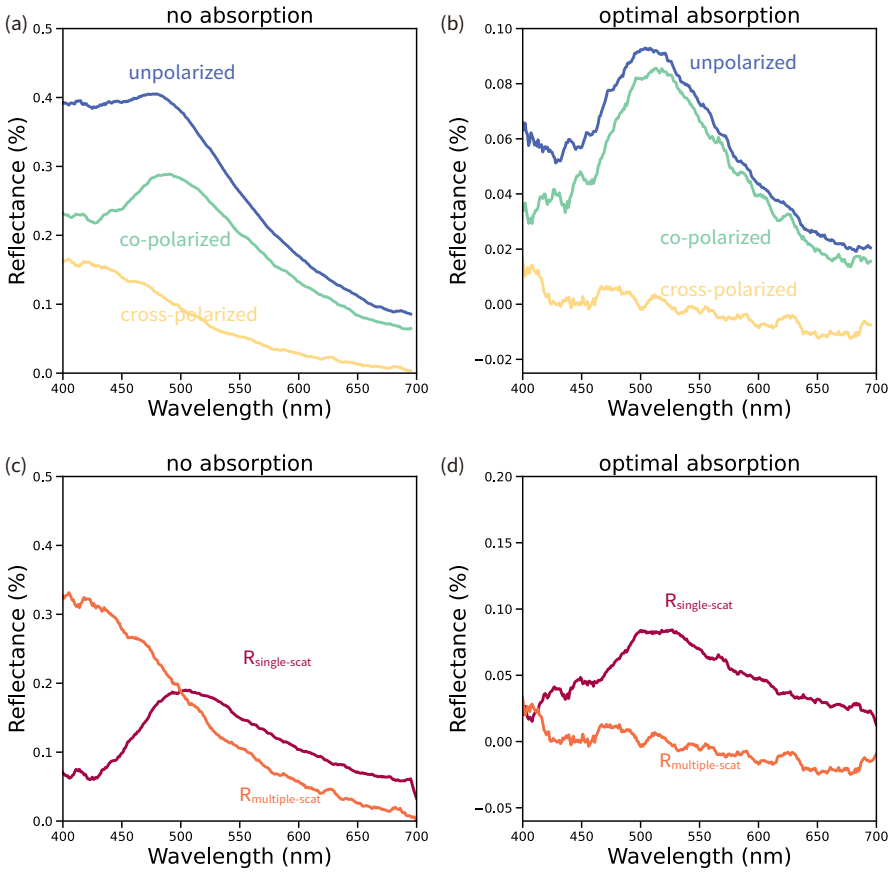

Fig. 11. (a,b) The unpolarized (blue), co-polarized (cyan), and cross-polarized (orange) reflection spectra of photonic glass film samples without absorption and with the optimal absorption. (c, d) The reflectance coming from single scattering and multiple scattering in samples without absorption and with the optimal absorption. In all measurements, the incident light is perpendicular to the sample surface and the angle between the incident light and the detector is 20°. The spectra are smoothed by averaging 10 adjacent sampling points.

There are two approaches to make particles with desired absorption. One is to coat a thin layer of absorbing materials onto nonabsorbing particles. The degree of absorption can be controlled by the shell thickness. For example, Liu et al. [17] have synthesized core-shell nanoparticles by coating a layer of absorbing polydopamine onto the surface of silica nanoparticles. With appropriate shell thickness, photonic glass films assembled from the core-shell nanoparticles show bright structural colors. The other approach is to tune chemical structures to make solid nanoparticles with different levels of absorption. Synthetic melanin-like nanoparticles are a great candidate for this purpose, since their absorption can be greatly adjusted by designing different donor-acceptor pairs or doping metal ions [51,52].

3.5. *Experimental validation of design rule*

To validate the design rule, we set to make photonic glass films assembled from silica nanoparticles with carbon black as absorber. To quickly identify the volume fraction of the sample made by a dropcasting method, we fit the volume fraction to match the simulated reflectance spectra with the experimental measure spectra. We find the volume fraction is 45% (Fig. S12). With the

Optics EXPRESS

diameter of silica nanoparticles (218 nm), their refractive index, and the volume fraction, we calculate the average transport mean free path of the sample $\overline{l^*} = 26.09\ \mu$m over 400-700 nm and obtain the optimal imaginary refractive index of the *sample*, $k_{\text{sample}} = 1.68 \times 10^{-3}$ at 550 nm by setting $\overline{l_a} = \overline{l^*}$. We then compute the optimal imaginary index of the *matrix* using Bruggeman equation, $k_{\text{matrix}} = 2.86 \times 10^{-3}$. Finally, the optimal volume fraction of carbon black in the matrix is calculated, $v_{\text{CB}} = k_{\text{matrix}}/k_{\text{CB}} = 6.5‰$.

We drop cast solutions of silica particles with different concentrations of carbon black to make photonic glass samples with tunable absorption. Guided by the design rule, we prepare samples with seven different percentages of carbon black relative to the matrix, including 6.5‰. As shown in Fig. 10, the reflectance intensity decreases and reflectance peak sharpens with a higher percentage of carbon black. With further increase in carbon black, the reflectance spectrum flattens. The color saturation of the sample increases from 0.22 to 0.38 and then decreases to 0.29. The sample with 6.5‰, calculated from design rule, has the saturation of 0.37, almost the same with the largest saturation of 0.38. This suggests that our design rule can efficiently identify the required amount of absorber to achieve highly saturated photonic glasses (Fig. S11).

To quantify how absorption affects the multiple scattering, we measure the reflection spectra of samples in different polarization modes. For the sample without absorption, both unpolarized and co-polarized reflectance spectra shows a reflection peak around 480 nm, but the co-polarized spectra has a sharper peak (Fig. 11(a)). The cross-polarized reflectance spectrum shows no peak with a higher reflectivity at short wavelengths. For the sample with the optimal absorption, the unpolarized and co-polarized spectra are much closer to each with a narrower peak. The cross-polarized spectrum decays to zero across the whole wavelengths.

Based on the fact that the polarization direction becomes randomized for the multiple scattering, we can isolate multiple scattering and single scattering from these polarization spectra (see details in Section 2.4). As shown in Fig. 11(c), the reflectance spectrum contributed by the single scattering has a clear peak, while the spectrum contributed by the multiple scattering has no peak with larger intensity at shorter wavelengths. Thus, the multiple scattering smears out the single scattering peak, decreasing the color saturation. With the optimal absorption, the multiple scattering is greatly reduced to almost zero (Fig. 11(d)) and the single scattering accounts for the main contribution to the reflectance spectrum. These results are consistent with our simulations that the optimal absorption minimizes the multiple scattering and the highest color saturation is achieved when the reflectance is majorly contributed by the single scattering.

4. Conclusion

In this work, we use validated multiple scattering model based on Monte-Carlo methods to investigate how adding absorption into the matrix affects the color saturation of photonic glasses. We find color saturation increases with absorption until it reaches a maximum at an optimal amount of absorption. The optimal absorption is independent on the sample thickness, but it varies with refractive index contrast. With higher index contrasts, there is stronger multiple scattering and more absorption is required to achieve the optimal saturation. When the absorption mean free path is comparable to the transport mean free path, the saturation reaches a maximum. This is because with such absorption, the multiple scattering is minimized and the reflectance is primarily contributed by the single scattering. We demonstrate that this finding serves as a design rule to determine the optimized absorption needed for making highly saturated photonic glasses. This will inform future experiments aimed at expanding the color gamuts of photonic glasses, paving the way for the widespread application of highly saturated, angle-independent structural colors. In addition, this work offers a better understanding of the interaction of light absorption and scattering in disordered correlated photonic systems.

Optics EXPRESS

Funding. National Natural Science Foundation of China (52203273); Sichuan Science and Technology Program (2023NSFSC0305); State Key Laboratory of Polymer Materials Engineering (sklpme2023-2-14); Fundamental Research Funds for the Central Universities.

Acknowledgments. We thank the Manoharan group for the source of multiple scattering model. We are grateful to Boxiang Wang, Shuhong Xiang, Dong Yang, Xiuhua Yang, Yujie Peng, Ruiming Jia, Hongyu Yan, Li Yang, Mengdi Chen for their valuable discussion and suggestions on the manuscript.

Disclosures. The authors declare no conflicts of interest. M. X. and Z. G. are authors on a pending patent related to this work filed by Sichuan University on March 08, 2024 (Patent Application Number: 202410259912.4).

Data availability. Data underlying the results presented in this paper are not publicly available at this time but may be obtained from the authors upon reasonable request.

Supplemental document. See Supplement 1 for supporting content.

References

1. J. Ballato, J. Dimaio, A. James, *et al.*, "Photonic band engineering through tailored microstructural order," Appl. Phys. Lett. **75**(11), 1497–1499 (1999).
2. J. Ballato, "Tailoring visible photonic bandgaps through microstructural order and coupled material effects in sio$_2$ colloidal crystals," J. Opt. Soc. Am. B **17**(2), 219–225 (2000).
3. P. D. García, R. Sapienza, Á. Blanco, *et al.*, "Photonic glass: a novel random material for light," Adv. Mater. **19**(18), 2597–2602 (2007).
4. P. D. García, R. Sapienza, Á. Blanco, *et al.*, "Photonic glasses: a step beyond white paint," Adv. Mater. **22**(1), 12–19 (2010).
5. V. Saranathan, J. D. Forster, H. Noh, *et al.*, "Structure and optical function of amorphous photonic nanostructures from avian feather barbs: a comparative small angle X-ray scattering (SAXS) analysis of 230 bird species," J. R. Soc. Interface. **9**(75), 2563–2580 (2012).
6. H. Noh, S. F. Liew, V. Saranathan, *et al.*, "Double scattering of light from biophotonic nanostructures with short-range order," Opt. Express **18**(11), 11942–11948 (2010).
7. M. D. Shawkey, V. Saranathan, H. Pálsdóttir, *et al.*, "Electron tomography, three-dimensional Fourier analysis and colour prediction of a three-dimensional amorphous biophotonic nanostructure," J. R. Soc. Interface. **6**(suppl_2), S213–S220 (2009).
8. I. Lee, D. Kim, J. Kal, *et al.*, "Quasi-amorphous colloidal structures for electrically tunable full-color photonic pixels with angle-independency," Adv. Mater. **22**(44), 4973–4977 (2010).
9. L. Bai, V. C. Mai, Y. Lim, *et al.*, "Large-scale noniridescent structural color printing enabled by infiltration-driven nonequilibrium colloidal assembly," Adv. Mater. **30**(9), 1705667 (2018).
10. Y. Takeoka, S. Yoshioka, A. Takano, *et al.*, "Production of colored pigments with amorphous arrays of black and white colloidal particles," Angew Chem. Int. Ed. **52**(28), 7261–7265 (2013).
11. Y. Xue, F. Wang, Y. Qin, *et al.*, "Angle-independent structurally colored PS@TiO $_2$ film with excellent underwater superoleophobicity in harsh environments," Langmuir **35**(21), 6956–6961 (2019).
12. A. F. Demirörs, E. Poloni, M. Chiesa, *et al.*, "Three-dimensional printing of photonic colloidal glasses into objects with isotropic structural color," Nat. Commun. **13**(1), 4397 (2022).
13. T. Yamanaka, N. Tarutani, K. Katagiri, *et al.*, "High heat resistance of the structural coloration of colloidal arrays with inorganic black additives," ACS Appl. Mater. Interfaces **14**(25), 29324–29330 (2022).
14. J. Chu, Y. Chen, S. Tan, *et al.*, "Edible amorphous structural color," Adv. Opt. Mater. **10**(4), 2102125 (2022).
15. Y. Zhang, B. Dong, A. Chen, *et al.*, "Photonics: using cuttlefish ink as an additive to produce non-iridescent structural colors of high color visibility," Adv. Mater. **27**(32), 4666 (2015).
16. Q. Guo, X. Wang, J. Guo, *et al.*, "3d printing of non-iridescent structural color inks for optical anti-counterfeiting," Nanoscale **15**(46), 18825–18831 (2023).
17. P. Liu, J. Chen, Z. Zhang, *et al.*, "Bio-inspired robust non-iridescent structural color with self-adhesive amorphous colloidal particle arrays," Nanoscale **10**(8), 3673–3679 (2018).
18. A. Kawamura, M. Kohri, G. Morimoto, *et al.*, "Full-color biomimetic photonic materials with iridescent and non-iridescent structural colors," Sci. Rep. **6**(1), 33984 (2016).
19. F. Li, B. Tang, J. Xiu, *et al.*, "Hydrophilic modification of multi-walled carbon nanotube for building photonic crystals with enhanced color visibility and mechanical strength," Molecules **21**(5), 547 (2016).
20. Y. Zhang, P. Han, H. Zhou, *et al.*, "Highly brilliant noniridescent structural colors enabled by graphene nanosheets containing graphene quantum dots," Adv. Funct. Mater. **28**(29), 1802585 (2018).
21. N. Sun, X. Liu, Y. Liu, *et al.*, "Enhancing the brightness and saturation of noniridescent structural colors by optimizing the grain size," Nanoscale Adv. **2**(10), 4581–4590 (2020).
22. J. Yu, C.-H. Lee, and C.-W. Kan, "Graphene oxide/reduced graphene oxide enhanced noniridescent structural colors based on silica photonic spray paints with improved mechanical robustness," Nanomaterials **11**(4), 949 (2021).
23. M. Iwata, M. Teshima, T. Seki, *et al.*, "Bio-inspired bright structurally colored colloidal amorphous array enhanced by controlling thickness and black background," Adv. Mater. **29**(26), 1605050 (2017).

Optics EXPRESS

24. M. Xiao, Y. Li, M. C. Allen, *et al.*, "Bio-inspired structural colors produced via self-sssembly of synthetic melanin nanoparticles," ACS Nano **9**(5), 5454–5460 (2015).
25. J. Wang, W. Chen, D. Yang, *et al.*, "Photonic lignin with tunable and stimuli-responsive structural color," ACS Nano **16**(12), 20705–20713 (2022).
26. Z. Lin, Z. Gong, D. Q. Bower, *et al.*, "Bidispersed colloidal assemblies containing xanthommatin produce angle-independent photonic structures," Adv. Opt. Mater. **9**(24), 2100416 (2021).
27. S. Magkiriadou, J.-G. Park, Y.-S. Kim, *et al.*, "Absence of red structural color in photonic glasses, bird feathers, and certain beetles," Phys. Rev. E **90**(6), 062302 (2014).
28. H. Noh, S. F. Liew, V. Saranathan, *et al.*, "Contribution of double scattering to structural coloration in quasiordered nanostructures of bird feathers," Phys. Rev. E **81**(5), 051923 (2010).
29. G. Shang, Y. Häntsch, K. P. Furlan, *et al.*, "Highly selective photonic glass filter for saturated blue structural color," APL Photonics **4**(4), 046101 (2019).
30. L. Maiwald, S. Lang, D. Jalas, *et al.*, "Ewald sphere construction for structural colors," Opt. Express **26**(9), 11352 (2018).
31. G. J. Aubry, L. Schertel, M. Chen, *et al.*, "Resonant transport and near-field effects in photonic glasses," Phys. Rev. A **96**(4), 043871 (2017).
32. L. Schertel, L. Siedentop, J. Meijer, *et al.*, "The structural colors of photonic glasses," Adv. Opt. Mater. **7**(15), 1900442 (2019).
33. A. Patil, C. M. Heil, B. Vanthournout, *et al.*, "Structural color production in melanin-based disordered colloidal nanoparticle assemblies in spherical confinement," Adv. Opt. Mater. **10**(5), 2102162 (2022).
34. C. M. Heil, A. Patil, B. Vanthournout, *et al.*, "Mechanism of structural colors in binary mixtures of nanoparticle-based supraballs," Sci. Adv. **9**(21), eadf2859 (2023).
35. V. Hwang, A. B. Stephenson, S. Magkiriadou, *et al.*, "Effects of multiple scattering on angle-independent structural color in disordered colloidal materials," Phys. Rev. E **101**(1), 012614 (2020).
36. V. Hwang, A. B. Stephenson, S. Barkley, *et al.*, "Designing angle-independent structural colors using monte carlo simulations of multiple scattering," Proc. Natl. Acad. Sci. **118**(4), e2015551118 (2021).
37. M. Xiao, A. B. Stephenson, A. Neophytou, *et al.*, "Investigating the trade-off between color saturation and angle-independence in photonic glasses," Opt. Express **29**(14), 21212 (2021).
38. A. B. Stephenson, M. Xiao, V. Hwang, *et al.*, "Predicting the structural colors of films of disordered photonic balls," ACS Photonics **10**(1), 58–70 (2023).
39. S. Magkiriadou, V. Hwang, A. Stephenson, *et al.*, "Structural-color-a python package for modeling angle-independent structural color," GitHub (2020), https://github.com/manoharan-lab/structural-color.
40. P. Yazhgur, G. J. Aubry, L. S. Froufe-Pérez, *et al.*, "Light scattering from colloidal aggregates on a hierarchy of length scales," Opt. Express **29**(10), 14367–14383 (2021).
41. P. Yazhgur, G. J. Aubry, L. S. Froufe-Pérez, *et al.*, "Scattering phase delay and momentum transfer of light in disordered media," Phys. Rev. Res. **4**(2), 023235 (2022).
42. C. F. Bohren and D. R. Huffman, *Absorption and scattering of light by small particles* (John Wiley & Sons, 2008).
43. G. A. Klein and T. Meyrath, *Industrial color physics*, vol. 154 (Springer New York, 2010).
44. W. Stöber, A. I. Fink, and E. Bohn, "Controlled growth of monodisperse silica spheres in the micron size range," J. Colloid Interface Sci. **26**(1), 62–69 (1968).
45. V. A. Markel, "Introduction to the maxwell garnett approximation: tutorial," J. Opt. Soc. Am. A **33**(7), 1244 (2016).
46. D. S. Wiersma, P. Bartolini, A. Lagendijk, *et al.*, "Localization of light in a disordered medium," Nature **390**(6661), 671–673 (1997).
47. P. Chylek, G. Videen, D. Ngo, *et al.*, "Effect of black carbon on the optical properties and climate forcing of sulfate aerosols," J. Geophys. Res. **100**(D8), 16325–16332 (1995).
48. G. A. d'Almeida, P. Koepke, and E. P. Shettle, *Atmospheric aerosols: Global climatology and radiative characteristics*, (A. Deepak Pub., Hampton, Va., USA 1991).
49. M. Atif, H. Z. Haider, R. Bongiovanni, *et al.*, "Physisorption and chemisorption trends in surface modification of carbon black," Surf. Interfaces **31**, 102080 (2022).
50. B. Zhang, Y. Chen, F. Wang, *et al.*, "Surface modification of carbon black for the reinforcement of polycarbonate/acrylonitrile-utadiene-tyrene blends," Appl. Surf. Sci. **351**, 280–288 (2015).
51. Y. Zou, X. Chen, P. Yang, *et al.*, "Regulating the absorption spectrum of polydopamine," Sci. Adv. **6**(36), eabb4696 (2020).
52. Z. Wang, Y. Zou, Y. Li, *et al.*, "Metal-containing polydopamine nanomaterials: catalysis, energy, and theranostics," Small **16**(18), 1907042 (2020).